Seismic loss assessment of existing hotel building in Ecuador

Jose Poveda , M.EERI(iD), and Gerard J O'Reilly , M.EERI(iD)

Abstract

This article presents results from a case study seismic assessment of an existing hotel structure located in Quito, Ecuador, using a practice-oriented story-loss-based assessment methodology. The building, constructed in the late 1950s and considered a city landmark, has undergone several renovations and repairs but has yet to be seismically retrofitted. A detailed building survey was conducted, and extensive data on structural layout, dynamic characteristics, and the damageable inventory was developed with the aid of Building Information Modeling. The building numerical models were compared against available ambient noise vibration measurements, and using the collected survey data, fragility and vulnerability functions were derived from non-linear dynamic analyses. The results showed that the building has a notable expected annual loss, primarily due to repair costs associated with nonstructural elements and contributions from potential collapse. Overall, the results provide a benchmark example for conducting seismic loss assessment of non-code-compliant and other vulnerable structures in Ecuador and the South American context in general.

Keywords

Loss assessment, seismic risk, fragility, ambient noise data, dynamic analysis

Date received: 20 December 2023; accepted: 3 October 2024

Introduction

Performance-based seismic assessment of existing buildings is inherently complex due to the diverse structural typologies, construction materials, and historical building practices worldwide. These structures often lack original design documents and are seismically vulnerable since they typically predate modern seismic design standards. Consequently,

Centre for Training and Research on Reduction of Seismic Risk (ROSE Centre), Scuola Universitaria Superiore IUSS di Pavia, Pavia, Italy

Corresponding author:
Gerard J O'Reilly, Centre for Training and Research on Reduction of Seismic Risk (ROSE Centre), Scuola Universitaria Superiore IUSS di Pavia, Piazza della Vittoria 15, 27100 Pavia, Italy.
Email: gerard.oreilly@iusspavia.it

assessments must rely on building-specific data, field surveys, and advanced analysis techniques to reduce the uncertainties associated with these historical constructions.

The Pacific Earthquake Engineering Research (PEER) Center has developed a fully probabilistic framework to estimate earthquake-induced damage and monetary losses (Federal Emergency Management Agency (FEMA) P-58, 2018), integrating seismic hazard analysis and structural response simulation. This methodology encompasses four stages: assessing site-specific ground motion hazards using probabilistic seismic hazard assessment (PSHA), evaluating structural response to compute engineering demand parameters (EDPs), predicting damage using fragility functions that relate EDPs with damage probabilities, and estimating economic losses based on repair costs. Moreover, a simplified version of PEER's methodology, referred to as story-loss-based assessment, generates functions between EDPs and economic losses (Ramirez and Miranda, 2009). Story-loss functions alleviate the computational load and help focus on the structural performance results. The present study utilizes this framework to assess an existing building, producing valuable and relatable information for property owners.

Performance-based methodologies provide a means to assess any typology by explicitly considering its inherent uncertainties, as described in FEMA P-58 (2018), for example, or in an implicit manner, such as American Society of Civil Engineers (ASCE)/SEI 41-17 (2017). Still, technical difficulties related to the specifics of the existing building may need to be addressed by local experts. The seismic vulnerability of existing buildings is a critical concern in regions with a history of high seismic activity, such as Ecuador. This article focuses on a relatively modern hotel with local historical, architectural, and cultural heritage significance. While it may be considered risk category II or normal occupancy buildings, as per ASCE/SEI 7-16 (2017) and NEC-15 (2014), respectively, there is no mandatory seismic retrofit ordinance for this type of structure in Ecuador and developing retrofit strategies to mitigate its collapse or demolition is not only a matter of safeguarding public safety, but also a matter of preserving cultural identity. Depending on local legislation, in this case Ecuador, the decision to retrofit usually rests with the building owner.

This article presents a case study seismic assessment of an iconic hotel situated in Quito, Ecuador. The building was constructed during the late 1950s and has undergone various modifications over the years, yet seismic retrofitting remains an unaddressed concern. The case study assessment presented here encompasses a detailed seismic hazard analysis with hazard-consistent ground motion selection following state-of-the-art approaches. Field surveys, material tests, and ambient noise vibrations were used to develop a nonlinear numerical model and perform multiple stripe analysis (MSA) to characterize EDPs and estimate losses due to required repair costs. To do so, a damageable inventory was compiled based on detailed knowledge available from the building owners and collaboration with local experts to construct story loss functions (SLFs). Furthermore, structural fragilities following ASCE/SEI 41-17 (2017) damage state definitions were constructed, as local legislation refers primarily to this document. Finally, seismic vulnerability functions and expected annual losses (EALs) were estimated, representing a key metric for decision-makers. Discussion of the results delves into the need for further research on the structural typology and developing proper strategies to reduce the risk of collapse and potential economic losses in this region. Through this case study, this article aims to provide a clear illustration of how detailed seismic loss assessment can be carried out on such buildings and provide valuable data and insights on structural behavior and loss accumulation in the region, which may be helpful to other practitioners.

Case study

The first step in a seismic loss assessment, before beginning the analysis stages, is assembling the building performance model. This model includes basic building data such as size, repair costs, replacement cost, and details of vulnerable structural components and assemblies, specifying their location, their demands during an earthquake, their vulnerability to damage, and the consequences, such as collapse potential and necessary repairs. In addition, it addresses vulnerable nonstructural systems, components, and contents, detailing their location, damage vulnerability, and the resulting hazards and repair needs. Over the years, the present case study has been examined from different perspectives, including historical, architectural, and structural values, resulting in the compilation of vast amounts of information. One might think that all the compiled information facilitates the use of detailed seismic assessments; nevertheless, there always seems to be missing information and a lack of budget to survey it. Therefore, this project was a candidate for the use of new tools to overcome these difficulties. The present section briefly describes the project and its relevant information, how the damageable inventory was built for its later use, and finally, a description of the structural model based on the available data.

Description of building

The building is part of a more extensive complex of structures of an elongated hotel in Quito, Ecuador (Figure 1). The main hotel building was constructed in the late 1950s, and later expansions were mainly attached to the northern side, with each block possessing a structural joint on the superstructure level. It initially comprised five architectural blocks with a constructed area of approximately 15,400 m^2. Visual inspections revealed several key structural characteristics for each block. In particular,

- North Block: This comprises a two-story mixed-use structure with reinforced concrete (RC) walls and steel beams at the ground floor level, steel trusses for the roof, and 15–20 cm solid concrete slabs for both levels. It mainly comprises rental event halls, lobbies, bathrooms, service corridors, storage rooms, and offices.
- Central Block: The central block, with two underground floors, seven stories, and an accessible terrace, is primarily constructed using RC. It features perimeter columns, concrete core walls for staircases and elevators, and 25 cm unidirectional slabs with embedded masonry blocks supported by embedded beams. Underground floors are used for hotel infrastructure such as equipment, services, storage rooms, employee canteen, and more rental event halls. The ground floor encompasses the reception, offices, and retail stores. Middle stories are used for hotel rooms, the top story is a restaurant, and the roof hosts the elevator equipment.
- South and South-South Blocks: Each block has an additional structural joint in the middle, resulting in a total of four structural blocks. These structures, each three stories high with one-half confined underground floor due to the slope of the terrain, were constructed using RC with either 25 cm unidirectional slabs with embedded masonry blocks or 20 cm solid slabs. In addition, no shear walls were present, but there were stiff infill panels framed by columns that do not conform with modern codes. These blocks are used mainly as hotel rooms, corridors, offices, or storage.
- Bungalow Blocks: Three independent one-story structures made of RC with 25 cm unidirectional slabs with embedded masonry block and stiff infills framed by non-
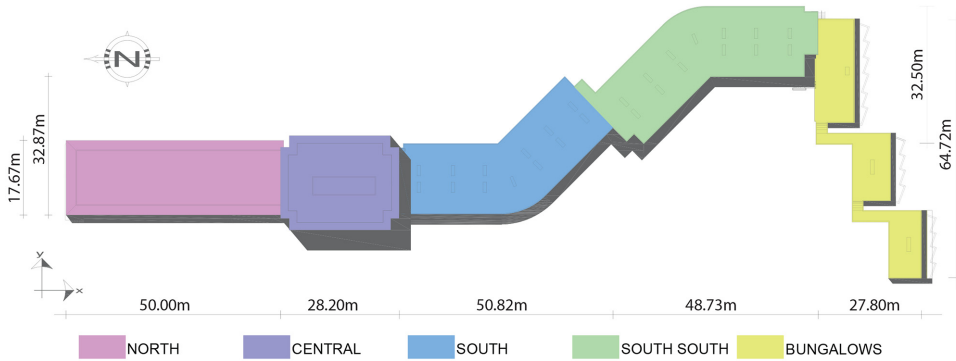
Figure 1. Plan distribution scheme of the various hotel blocks.

conforming code columns. These blocks serve as small apartments for short-term rental.

It is important to mention that amenities such as gardens, pools, saunas, and parking lots are on the building's exterior; hence, they are not described. Moreover, in all the structural blocks, most of the columns and walls' strongest axis (longest dimension) is in the Y-direction, or E-W direction, depicted in Figure 1.

Information on soil properties, material strength, typical reinforcement details, and ambient noise vibrations were collected by local experts via in situ surveys, archival research, and numerical analysis. No structural plans were available, so concrete core samples and steel scanning with calibration patches were used to determine the main structural elements' composition. The reported date of the beginning of project development was 1951, the same year the first Ecuadorian building code was published because of the Mw6.8 Ambato earthquake. It is logical to assume that it was most likely not seismically designed. Nevertheless, international professionals were involved, and common practice at the time included designing for gravity loads and a minimum lateral load, as was typical in other parts of the world, such as the early seismic provisions introduced in California after the 1933 Long Beach earthquake. It is curious to note that following discussions with local experts on past construction practices used in the region around this time, strong similarities with Italian and American construction practices were noted. This was due to the lack of sufficiently trained local engineers at the time, meaning that the influx of skilled migrants also meant importing their know-how. Following a detailed survey of the case study hotel building, notable differences compared to modern structures were found, including the use of smooth reinforcement bars, wider spacing of stirrups (>20 cm), bar overlaps in areas near joints, and a lack of specific considerations for joint connections. Such structures are categorized as highly vulnerable by more straightforward assessments such as Tier 1 and Tier 2 on ASCE/SEI 41-17 (2017), and limited ductile behavior is expected during seismic loading.

The present study was limited to the central block shown in Figure 2a primarily due to computational constraints; however, the study's relevance remains valid because the building concentrates on the essential functions and infrastructure of the hotel. Moreover, structural joints between the individual building blocks ranged from 4 to 8 cm allowing a decoupled modal structural analysis; therefore, the impacts of pounding were not
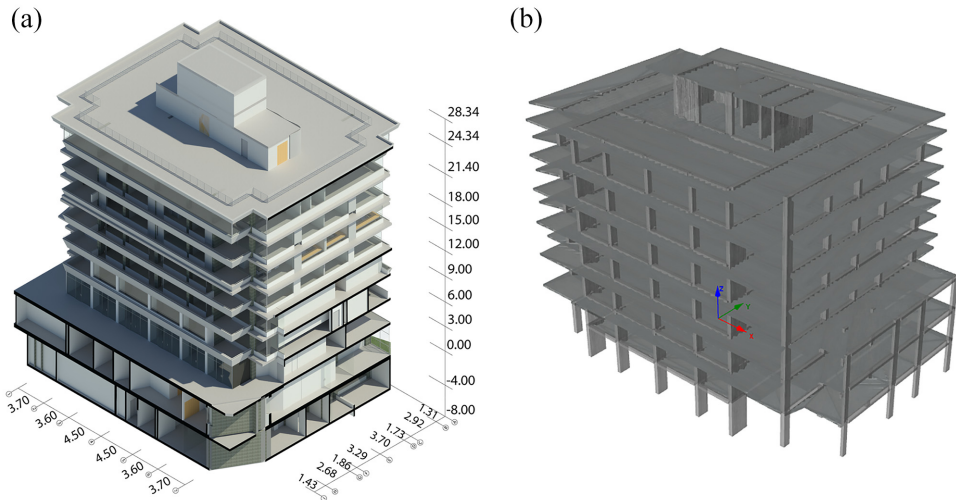
Figure 2. Illustration of the (a) architectural layout and (b) structural modeling of the case study block.

considered in the numerical analysis. The presence of these gaps also allowed the central block to be considered individually, since the modeling and analysis of the entire complex was found to be too computationally demanding. Furthermore, fixed-based behavior at ground level was assumed due to the relatively high stiffness of the underground floors provided by the basement walls, so only above-ground levels were considered for the analysis, as shown in Figure 2b.

Damageable inventory and repair costs

To illustrate how a more refined but expedited loss assessment can be implemented within this context, a damageable inventory was developed from the available documents and field surveys, similar to other recent studies such as Nafeh and O'Reilly (2023). In parallel, a detailed three-dimensional (3D) model was generated to facilitate building information modeling (BIM) integration. This was key for visualizing and grouping components together and then estimating their respective quantities. As an illustrative example, Figure 3 presents a plan view of the hotel's fourth story next to a 3D view with a color labeling of the partition walls.

The damageable inventory comprised data related to the non-structural elements (NSEs) like mechanical and electrical equipment, piping, partition walls, contents, sanitary units, and façade elements. The BIM integration proved to be very effective in grouping and identifying component groups and quantities, facilitating the interaction with the local experts to identify refined estimates of repair costs. A systematic categorization approach was employed to manage this extensive catalog of elements effectively. Initially, the inventory was organized into two categories: structural and non-structural. Due to the NSE inventory's complexity and size, a further sub-grouping of NSE was developed, recognizing the similarity between NSE and fragilities. In particular,

- Doors were classified into exterior, interior, or emergency types, reflecting their distinct functions and similarity in repair or replacement cost.
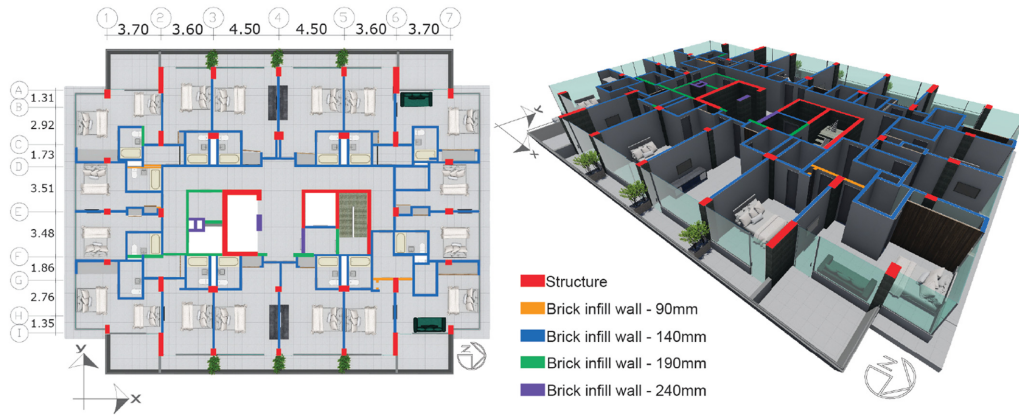
Figure 3. BIM model with the grouping of partition walls.

- Copper pipes were grouped in 3/4″, 2″, and 4″ diameters to reduce additional trivial categories with minor price differences, and their accessory costs were included in their unit price.
- PVC pipes were grouped in 110 and 200 mm diameters, and the accessory costs were included in their unit price.
- Steel pipes were considered a single 4″ category since the specific pipes currently used are no longer available, so a corresponding modern equivalent was considered.
- Gypsum and brick infill were differentiated by their thickness due to considerable price variability.
- Glazing was considered a single-element piece even if combined with prefabricated wood panels because its price incidence could be included in the unit price.
- Mechanical and electrical equipment were considered independently due to their price variations and acknowledging that repair or replacements in most cases would not be possible due to market availability, so equivalent modern equipment prices were considered.
- Electric connections such as cables and accessories were only considered replacements since most are not repairable after the infills fail.
- Room content replacement values were assigned according to their respective use, where a unit area price model was adopted since, when speaking with local experts, developing a detailed catalog of contents appeared to be a futile effort due to ever-changing styles and tastes, and a general budget model seemed more fitting with actual decorating and furnishing practice.

This grouping strategy enhanced the usability and clarity of the inventory, ignoring small variability that would make the exercise much more cumbersome with little return. Moreover, fragility functions characterizing each element's seismic vulnerability were defined using several sources, including FEMA P-58 (2018), research documentation, and expert opinion, detailed in Table 1. In particular,

- A single damage state was considered and directly correlated to the infills' collapse fragility for all doors, glazing and bathroom contents.

Table 1. General information on the damageable inventory catalog

Description	Source	Cod.	EDP	Repair cost unit
Non-conforming moment frame with inadequate development of reinforcing	FEMA P-58 (2018)	B1041.132b	PSD	Unit (per node)
Low-rise RC walls with return flanges	FEMA P-58 (2018)	B1044.043	PSD	m^2
Monolithic cast-in-place stairs with no seismic joints	FEMA P-58 (2018)	C2011.021b	PSD	Unit
Gypsum infill wall	FEMA P-58 (2018)	C3011.001a	PSD	m^2
Brick infill wall	Cardone and Perrone (2015)		PSD	m^2
Glazing	User		PSD	m^2
Doors (interior, exterior, emergency)	User		PSD	m^2
Bathroom contents and electric connections	User		PSD	m^2
RC parapet	User		PFA	m^2
Piping systems—water distribution	FEMA P-58 (2018)	D2021.011a	PFA	m
Sanitary waste piping	FEMA P-58 (2018)	D2031.011b	PFA	m
Vapor piping distribution	User	D2061.011a	PFA	m
Piping systems—gas distribution	User		PFA	m
Elevator/pre-1976	FEMA P-58 (2018)	D1014.012	PFA	Unit
Transformation chamber	FEMA P-58 (2018)	D5011.011a	PFA	Unit
Distribution panel	FEMA P-58 (2018)	D5012.031a	PFA	Unit
HVAC galvanized sheet metal ducting	FEMA P-58 (2018)	D3041.011a	PFA	kg
HVAC fan independently supported but not on vibration isolators	FEMA P-58 (2018)	D3041.002a	PFA	Unit
Equipment	User		PFA	Unit
Contents	User		PFA	m^2

- Balcony parapets were considered independent due to their weight and geometry. Fragilities were derived from a simple structural analysis of an equivalent cantilever beam.
- Mechanical equipment fragility was derived from expert opinion when equipment showed failure or overturning.
- The elevators are pre-1976 traction elevators, with fragility estimated as a function of peak floor accelerations (PFAs). While this simplifies reality, it is important to note that these complex electromechanical systems can also sustain damage from peak story drift (PSD) ratios, affecting components such as car guide rails, counterweight guide rails, and doors, which were not considered here.
- Contents were assigned a single damage state triggered by the leakage of piping that causes flooding. This assumption is crucial because it implies that the replacement of the contents results from indirect water damage caused by the piping damage, rather than from direct demands imposed on them. Typically, direct damage would be associated with peak floor velocity demands that cause toppling and slight damage to contents. However, it is assumed that replacement of the contents will only be necessary if there is water leakage on them. This assumption is significant because it means content replacement is determined by the performance of another element, rather than by the direct demands the contents themselves experience.

Finally, repair and replacement costs were compiled by a local expert, who conducted a detailed pricing analysis for the building's specific units and country contexts. This database fits better than the consequences database from other regions when local data is

unavailable or collected. This inventory provides actual data, which is enriched by understanding the as-built conditions of the structure under investigation. Table 1 presents a summary of the catalog and an extended version can be found via an electronic supplement. Each item is listed as being sensitive to one of the two EDPs considered here: PSD, defined as the relative lateral displacement of each story normalized by the story height, and PFA.

Numerical modeling

The numerical modeling of the hotel building was carried out using commercial software Seismosoft to assess structural behavior. For the steel reinforcement, the Menegotto-Pinto material model, characterized by a degraded strength $f_{s-deg} = 210\ MPa$ derived from ASCE/SEI 41-17 (2017) 10.3.5 guidelines based on expected yielding stress $f_{y,e} = 318\ MPa$ (grade 40), was determined from local expert recommendations. This reduction represents the stress at slippage of smooth bars with shorter development length l_d. The elastic modulus was assumed as $E_s = 200 GPa$ and a 0.5% post-yielding stiffness was used. It is noted that limited information was available for the rebar since no destructive tests were performed; lap splice length and location were assumed to be the worst case but were not systematically verified in situ. For the concrete, the Mander et al. (1988) material model was used, considering concrete elastic modulus $E_c = 25 GPa$ and an expected compressive strength of $f_{c,e} = 30\ MPa$, verified with destructive and non-destructive tests performed in situ. For the confinement of the core and cover concrete materials, a factor of $k = 1$ was defined since no seismic details and widely spaced hoops were observed in situ. The numerical model utilized force-based elements for the beam, column, and wall elements to model the structural members. For columns and beams, a plastic hinge length of 16% of the element length was defined (Scott and Fenves, 2006). This choice is standard practice and represents the observed plastic hinge lengths in laboratory tests and post-earthquake field inspections (Calabrese et al., 2010). A full-length distributed plasticity for the elements to ensure a general representation of their response was employed for walls. Shear-flexure interaction and shear failure modes were not directly accounted for, as preliminary analysis on the relevant strengths indicated that flexural yielding was the governing failure mode. The shear response of the walls was modeled elastically, and the shear capacity of the elements was estimated according to ACI Commitee 318 (2019). To account for the possible shear failure and sudden loss of vertical load-carrying capacity, the shear demands were checked during the post-processing of analysis results. This allowed non-simulated modes of failure to be identified and accounted for in the development of the collapse fragility function. The floor slab was modeled as a rigid diaphragm. The embedded one-way beams were modeled as identified in the field for the rotational stiffness contribution to the building and vertical load distribution. Fully rigid end offsets were assigned just to the beam ends half the size of the column, a distance between 15 and 30 cm, to account for the joint stiffness contribution. Still, no joint failure was modeled or expected based on a simple strength hierarchy verification carried out for the structure. In addition, rigid links between linear segments of the core walls, such as those found in stairwells and elevators, were assigned to realistically capture their interaction since they were monolithically built. Nonstructural components were not explicitly modeled in the analysis and their damage was considered through the evaluation of fragility functions, discussed later.

Ambient noise vibration measurements were also conducted on this building with Ref Tek 160-03 sensors with three 2 Hz seismometers and a triaxial accelerometer. While this was performed by a third-party contractor, meaning a full dataset was not available, some
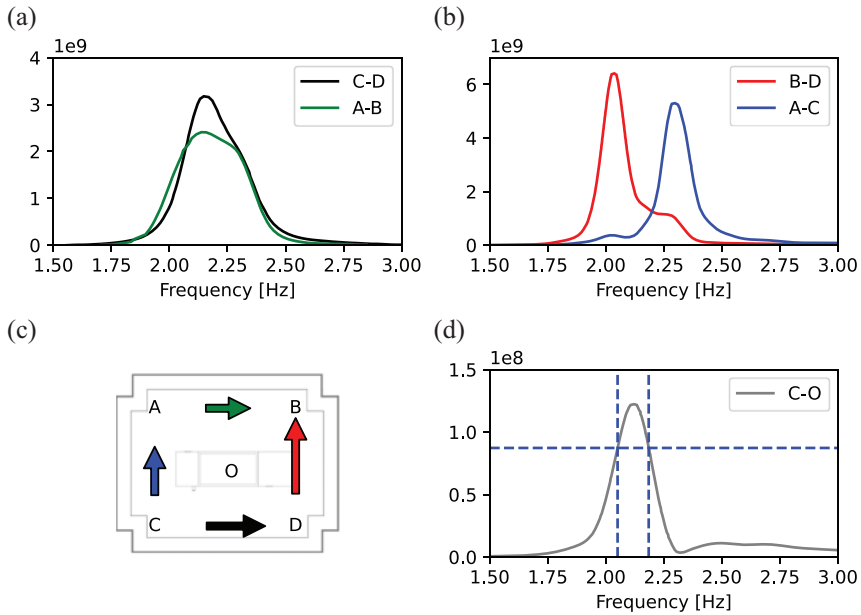
Figure 4. Spectra for top floor sides in (a) N-S and (b) E-W direction, (c) first mode amplitude scheme of top floor sides, and (d) first mode half-power bandwidth viscous damping.

general information was available and provided some information on the structure's modal response and equivalent viscous damping ratio. Five sensors were placed at the four corners in plan and the center, on the top floor and at other intermediate levels. Figure 4a and b presents the building transfer functions at the top floor in N-S and E-W directions, respectively. From these, it is first possible to observe the two first mode frequencies in the E-W direction. These are around 2 and 2.3 Hz, as seen in Figure 4b. In the N-S direction, the two peaks in the transfer function overlap and are similar in magnitude, making them harder to identify from the available data. The interpretation of the transfer functions indicates a torsional response, as depicted in Figure 4c, which shows indicatively via the arrow sizes how the side B-D displaces relative more than side A-C for the first mode. Moreover, the same torsional behavior was found in the numerical model. Figure 4d shows how the half-power bandwidth method was applied to estimate the first mode viscous damping.

In parallel, modal analysis was performed using the numerical model and compared with the ambient noise vibrations, which are listed in Table 3 accompanied by the two deformed mode shapes presented in Figure 5 which are in good agreement with Figure 4 results. Modal period results showed good agreement with the measured dynamic properties with a 20%–30% variation that may be attributed to differences in stiffness (i.e. infills) or in mass. Furthermore, the deformed shape of the controlling modes shapes can be verified from the ambient noise vibration. It is interesting to note, as shown in Table 2, that Mode 1 has a 46.31% effective modal mass in the X-direction and 11.88% in the Y-direction, and Mode 2 has a 5.99% effective modal mass in the X-direction and 48.7% in the Y-direction. Both are not widely spaced, which required additional effort to distinguish between the two structural periods in one direction. The damping values measured from the in situ measurement are also reported in Table 3. The damping ratio estimated using

Table 2. Effective modal mass percentage

Mode	Period [s]	U_x	U_y	R_z
1	0.63	46.35%	11.85%	8.23%
2	0.56	5.98%	48.75%	10.55%
3	0.48	13.29%	2.45%	53.84%
4	0.16	5.65%	0.38%	10.35%
5	0.12	6.68%	13.69%	0.90%
6	0.11	8.82%	7.73%	5.14%

Table 3. Modeled and measured structural vibration periods and damping ratios

Mode	Modeled period	Measured period	Measured damping ratio	Description
1	0.63 s	0.48–0.50 s	1.8%–3.5%	Mainly translational in X, rotation in Y
2	0.56 s	0.45–0.48 s	1.6%–3.0%	Mainly translational in Y, rotation in X
3	0.48 s	0.42–0.43 s	N/A	First torsional mode

the half-power bandwidth approach showed damping values in the 1.6%–3.5% range, slightly lower than the typically assumed value of 5% or 4.7% estimated by a regression function of height proposed by Cruz and Miranda (2021) from earthquake measurements. It is important to note that the half-power bandwidth method has been commonly used in the past and systematically overestimates the true damping ratios, as has been shown by Tamura et al. (2004), Kijewski-Correa and Pirnia (2007), and many others. For the numerical analysis, a Rayleigh damping model was defined with a 4% damping ratio for the first mode and a 6% damping ratio for the third mode. Slightly higher values from the observed were modeled since not all sources of dissipation were considered (i.e. internal partitions).

In addition to the modal analysis, a static pushover analysis was performed proportional to the modal shapes in Figure 5. The building was pushed in both orthogonal and opposite loading directions (i.e. positive and negative) as per ASCE/SEI 41-17 (2017) basic recommendations, allowing it to capture response proportional to its dynamic properties. The results, presented in Figure 6, help understand the nonlinear behavior and overall capacity of the structure. A normalized base shear coefficient, dividing by a total weight of 38,396.4 kN, and a roof drift, dividing by a total height of 24.5 m, are also presented. The base shear capacity is nearly 13% of the total weight in the X-direction and 10% in the Y-direction, which is typical of structure's with no lateral seismic design provisions. Pushover analysis was performed up to 2.5% of the total roof drift, which showed a smoothed yielding behavior with good numerical stability. It may be noted that the pushover curve in the Y-direction differs in the positive and negative direction; this effect might come from the torsional response in the E-W direction previously noted. Also illustrated in Figure 6 is the shear capacity of the walls in either direction, which are seen to be double in magnitude above the base shear demand, indicating that shear failure was not the critical mechanism. It is important to note that the numerical model retains lateral capacity since no shear failure mechanism was considered and this was modeled as elastic. Nevertheless, collapse is later checked during the post-processing of the dynamic analysis results and it was noted that this occurred at a drift value lower than the maximum value shown in the pushover.
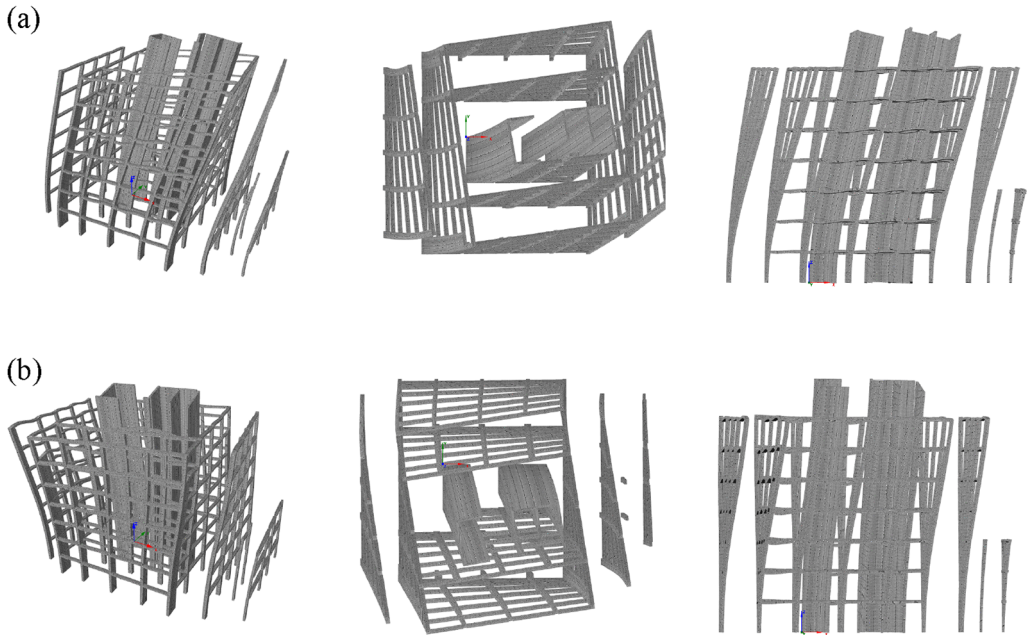
(a)

(b)

Figure 5. Perspective, upper, and front view of deformed shape for (a) mode 1 and (b) mode 2 obtained from the numerical model.
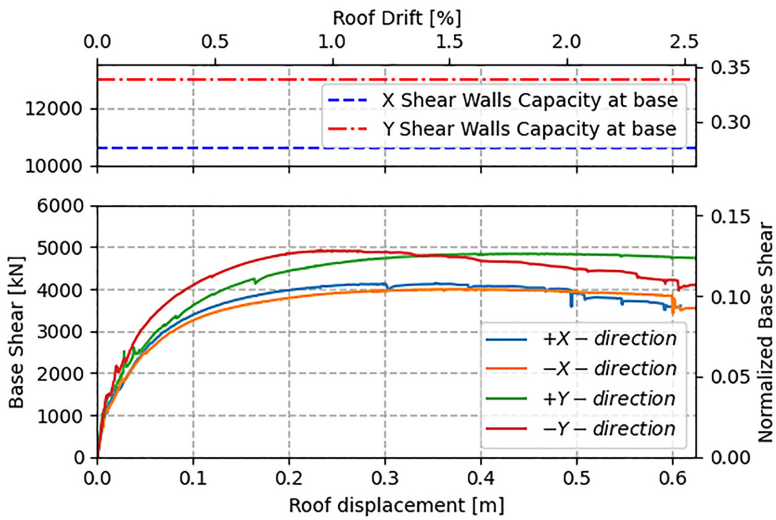

Figure 6. Static pushover analysis results for building analysis in both orthogonal and opposite loading directions.
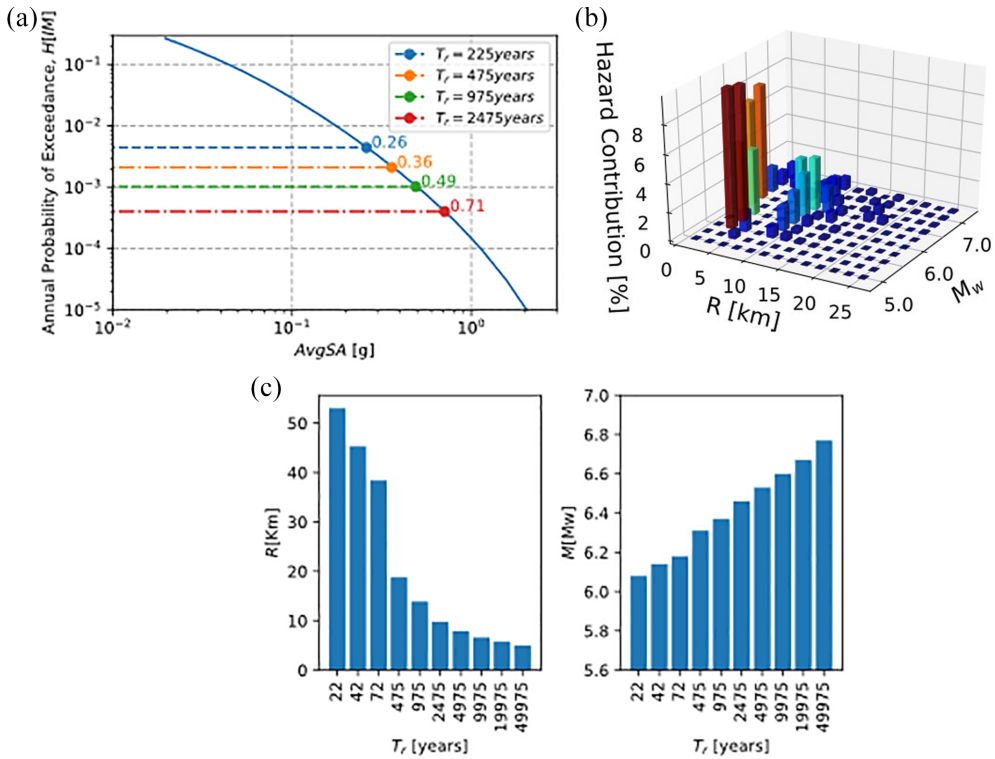
Figure 7. (a) Seismic hazard curve, (b) disaggregation information for 975 years, and (c) summary of R and M at the site location in Quito, Ecuador.

Analysis

Seismic hazard and ground motion record selection

PSHA characterizes earthquake ground motion with an intensity measure (IM), usually spectral acceleration at a given period of vibration, *T*. For nonlinear response history analysis, shaking effects are assessed by simultaneously evaluating responses to orthogonal pairs of horizontal ground motion components. These ground motion pairs are scaled to be consistent with the target response spectrum for a given return period.

A PSHA was performed in OpenQuake (Pagani et al., 2014) utilizing the Beauval et al. (2018) seismic hazard model and updating its catalog with recent earthquakes in the region. The seismic hazard curve for the site location in Quito, Ecuador, is shown in Figure 7. This was obtained by applying the indirect method described by Kohrangi et al. (2018) to compute hazard curves in terms of an IM termed average spectral acceleration, *AvgSA*, which has been shown to be quite advantageous and improve accuracy. The period range to define *AvgSA* spanned from $0.2T^*$ to $3T^*$, as in Eads et al. (2015), where $T^* = 0.6\ s$ is the mean between fundamental periods in the longitudinal and transverse directions, $T_{X,1} = 0.63\ s$ and $T_{Y,1} = 0.56\ s$, of the model of the structure. A $V_{s,30} = 480\ m/s$ obtained from in situ soil standard penetration tests was used in the model to account for local soil effects. Four different return period values are shown in Figure 7a to understand the intensity values at code-required return periods for building assessments in Ecuador.
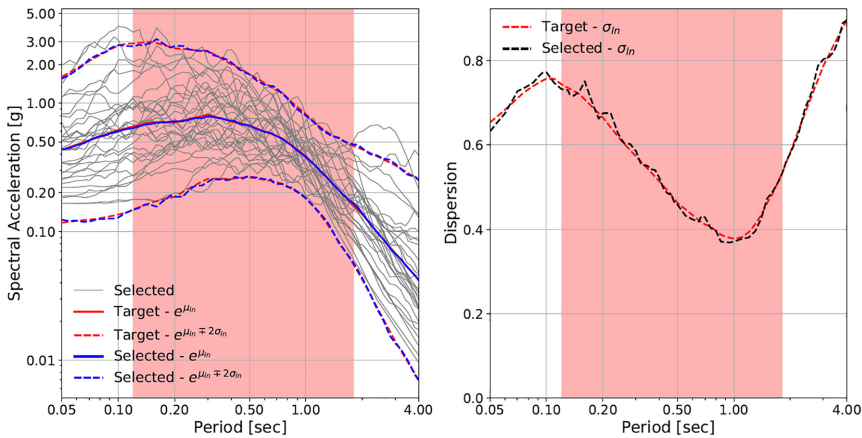
Figure 8. Target conditional spectrum and selected ground motion records.

Disaggregation for ten return periods spanning from 22 to 49,975 years was performed to estimate the magnitude, M, and rupture distance, R, parameters for constructing conditional spectra and record selection (Baker, 2011). Figure 7b showcases the 975 return period's complete disaggregation and Figure 7c also shows the mean values for each return period, in which R ranged from 53.0 to 5.0 km, and M ranged from 6.08 to 6.77 Mw. Interestingly, the dominant scenario for most of the analyzed return periods is from sources less than 20 km away, which is the intra-slab failure system that crosses the city of Quito. Record selection was performed using python-based code Djura Record Selector using the NGA-West2 database (Ancheta et al., 2014). A total of 30 records were selected for each return period with a maximum scale factor of 2.5 and minimum of 0.4. Figure 8 shows the record selection for the 475-year return period and how its mean exhibits good agreement with the mean and variance of the conditional spectrum based on spectral acceleration only, with other aspects like cumulative IMs not considered here. Again, the list of records and scale factors are available as an electronic supplement at https://gerard-joreilly.github.io/publications/.

Multiple stripe analysis

Structural analysis evaluates a building's response to earthquake shaking and estimates structural response parameters to estimate structural and nonstructural damage. Key response parameters include floor accelerations, story drift ratios, and residual drift ratios. These demands are used to develop statistics, including median values and dispersions, and to derive correlations between different demands. Hereafter, the so-called time-based assessment (FEMA P-58, 2018) is now presented as MSA.

Using the records selected for each intensity level, non-linear time history (NLTH) analysis was performed via MSA (Jalayer, 2003). The benefits of MSA instead of other well-established techniques, such as incremental dynamic analysis (IDA) proposed by Vamvatsikos and Cornell (2002), are the compatibility of record selection with site hazard features via the conditional spectrum approach and the possibility of using limited scale factors for all intensity levels (Baker, 2015), helping avoid problems of response bias recently reported in the literature (Dávalos and Miranda, 2019). Results for displacements
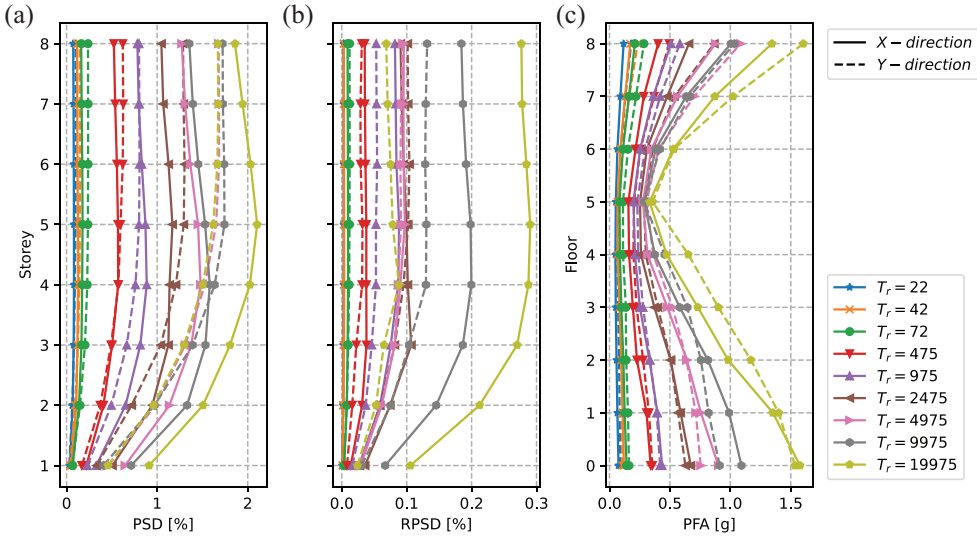
Figure 9. (a) Median peak story drift (PSD) (%), (b) residual peak story drift (RPSD) (%), and (c) peak floor acceleration (PFA) (g) profiles at increasing return periods.

and accelerations were recorded at the structure's center of mass, and PSD and PFA for each building level were computed. Residual peak story drift (RPSD) was also estimated, allowing the structure to vibrate freely after the ground motion record ended. The structural collapse (C) was defined as exceedance by 1.5 times the collapse prevention (CP) drift capacity, as per the structural backbone definition outlined by ASCE/SEI 7-16 (2017), or when numerical non-convergence was reached.

The median EDP profiles are shown in Figure 9 for each considered intensity and structural direction conditioned on no collapse. Interesting to note is that the highest return period generates 100% collapses and is therefore not shown. We can see from the PSD profiles that the X-direction is slightly more flexible and has higher drifts, consistent with the period measurements and stiffness distribution on elements discussed earlier. Figure 9 also presents the mean RPSD for the non-collapsed cases, which were estimated based on free vibration following the ground motion. Another approach could have been to estimate this residual drift from empirical relationships as a function of peak drift, since FEMA P-58 (2018) has suggested that free vibration measurements can be sensitive to modeling assumptions. Given the lack of specific data for this typology and region, the free vibration approximation was adopted but the limitations of this approach are noted here nonetheless. Examining the RPSD values in Figure 9b shows that some residual drifts would be observed at the 475-year shaking, despite the modest level of peak drift demands during shaking, which were around 0.6%. When comparing these drift demands to the approximate yield point shown in Figure 6, it can be seen that some degree of nonlinear behavior occurs, which in turn causes this residual deformation. Likewise at the higher return periods, where notable residual deformations are observed and in line with thresholds noted to be significant to occupants in studies like McCormick et al. (2008), for example. Regarding PFA, it is possible to see some amplification on the top floors with reduced demands at mid-height, illustrating the multi-modal contributions to the PFA demands.
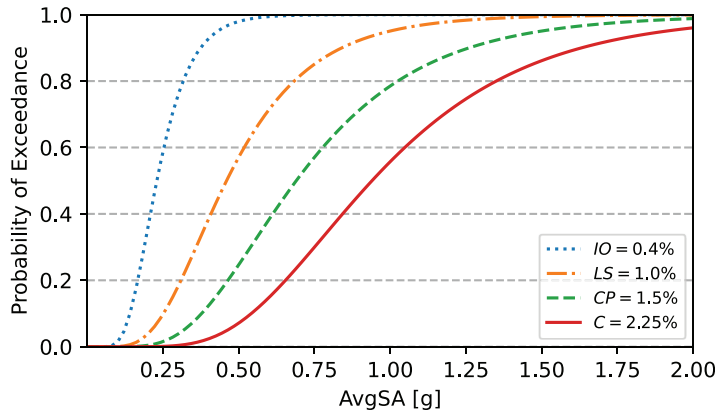
Figure 10. Fragility functions, corresponding median, and dispersion values: $\theta_{IO} = 0.23$, $\beta_{IO} = 0.38$, $\theta_{LS} = 0.46$, $\beta_{LS} = 0.47$, $\theta_{CP} = 0.69$, $\beta_{CP} = 0.47$, and $\theta_C = 0.94$, $\beta_C = 0.43$.

These acceleration peaks in the upper floors are due to higher mode effects, yielding at the base and vertical stiffness structural irregularity.

Fragility functions

The fragility functions presented in Figure 10 were developed by fitting a cumulative distribution function for the probability of exceedance of the different damage states that control the structural response, which in this case was the shear wall response. The first three damage states of the shear walls were defined as per ASCE/SEI 41-17 (2017) acceptance criteria tables for PSD-sensitive elements known as Immediate Occupancy (IO), Life Safety (LS), and Collapse Prevention (CP), in addition to the collapse (C) limit state, this drift percentage values are 0.4%, 1.0%, 1.5%, and 2.25%, respectively. At this point, it is possible to quickly note that the structure would likely satisfy the code-based assessment since median capacity values for LS and CP exceed 0.26g and 0.49g *AvgSA* intensities corresponding to 225 and 975 years return periods, respectively, as performance objectives for existing structures. Moreover, the collapse probability for the 975-year return period does not exceed the 10% threshold, as stated in the ASCE/SEI 7-16 (2017) provision. On the other hand, a 10% collapse probability is exceeded for the 2475-year return period intensity if it were to be assessed as a new structure. Hence, if assessed as an existing structure, it is not problematic, but if it were considered a new structure, it would be. Seismic collapse risk is computed as the annual rate of structural collapse by combining the hazard curve with the collapse fragility. Integrating the two, the mean annual frequency of collapse (MAFC) was found to be $\lambda_C = 0.375\text{e-}3$, corresponding to a return period of 2664 years. The MAFC is considerably larger (i.e. more frequent) than the limit suggested by ASCE/SEI 7-16 (2017) for new structures, which is 1% in 50 years, which corresponds to a 5000-year return period.

Derivation of SLFs

SLFs were generated following the procedure described by Shahnazaryan et al. (2021), which followed previous work by Ramirez and Miranda (2009) and Papadopoulos et al. (2019). Monte Carlo simulations were performed to generate a loss function for each
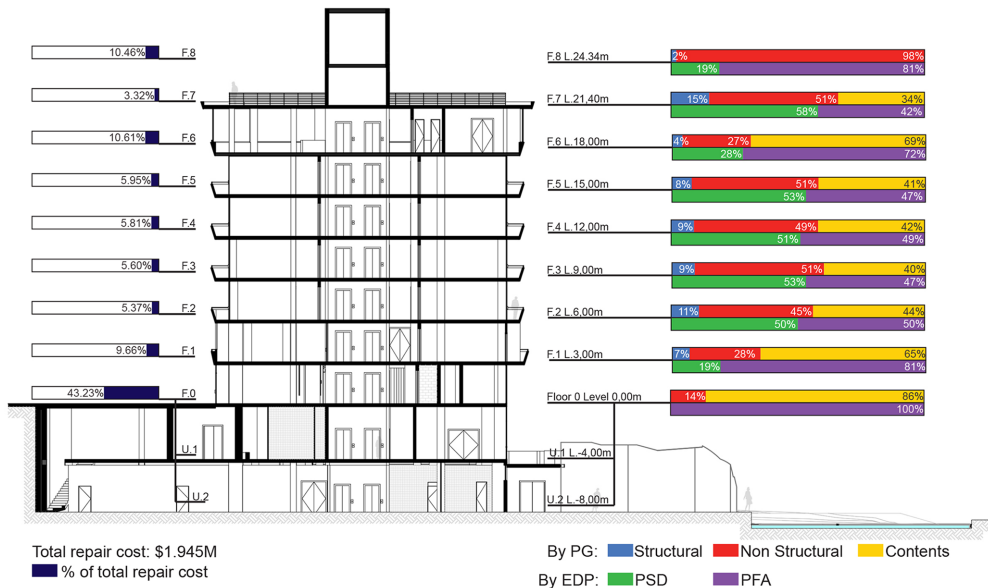
Figure 11. Distribution of the total repair costs among each story in terms of Performance Group and EDP.

story. A total of 20 realizations of damage and repair costs were sampled for each component of the performance groups, and the costs were summed to obtain the total loss of the performance group for a given EDP. In this case, PSD and PFA were the selected EDPs since they are the most common and have available fragilities in the literature for the NSEs. For the specific case of the underground floors catalog, PSD- and PFA-sensitive components were lumped into the corresponding ground floor catalog for simplicity as no great variation in their demands was anticipated among the different levels. PSD-sensitive components were discarded since no significant underground drift was expected nor modeled, in addition to the value of these components being relatively small. All damage was assumed to occur in the vertical elements as a result of these lateral demands in either direction. To better illustrate the repair cost distribution throughout the building height, Figure 11 shows the overall value of the total repair costs for each story and the percentage distribution per performance group (PG) or EDP sensitivity. It is noted that the terms PSD and PFA refer to the peak values over time of a ground motion, meaning that there is a distinct value for each level of the building. From the repair cost distribution, it is possible to underline the relatively high value that NSE and contents have compared to the structural repair cost at the different stories. A similar proportion between structural and non-structural components was shown by Taghavi and Miranda (2003) for the hotel typology. Moreover, since the ground floor and underground floors have a larger area and costly equipment required for the general operation of the entire hotel building complex, the ground floor has the most significant repair cost value. It is seen that this is entirely due to the PFA-sensitive damage, further supporting a decision to either protect this valuable machinery with dampers or base isolation, for example.

Following the Monte Carlo simulation, a Weibull function is fitted for each EDP and story, acknowledging this assumption is based on previous work by Shahnazaryan et al.

(2021), and may not always be the case since SLFs may not always be S-shaped. Figure 12 shows the SLFs for PSD-sensitive components for each structural orthogonal direction separately and the corresponding SLF for PFA-sensitive losses. In the case of the PSD-sensitive SLFs, one direction has a higher repair cost value. This is explained by the fact that one-direction loading systems were standard for the typology and construction date under consideration. Moreover, most areas of strong infills coincide with the stiff direction of the columns, increasing the repair costs of the specific direction due to the increased PFA demands that damage the nonstructural components. It is seen that there tends to be a degree of variability between the SLFs produced for each individual level, with some having different shapes and magnitudes. This is not deemed problematic but rather a consequence of the non-uniformity in the damageable components and their EDP sensitivity. Should practitioners deduce from Figure 11 which story best reflects their situation, that SLF may be used. Regarding the PFA-sensitive SLF, it is evident that the ground floor represents a significant repair cost, given the location of valuable building equipment. Comparing losses of both types of EDPs, PFA losses are considerably higher than PSD losses. Another major contributor is the assumption that many building contents are assumed to be correlated to damage to the piping fragilities, which was previously discussed. Their damage and assumed replacement is therefore caused by excessive damage and subsequent leakage of the piping is considered to trigger extensive contents replacement across the building, instead of a direct estimate of the demands on the contents themselves. It is believed that this assumption is a fair reflection of reality, considering this exact situation has been observed in past earthquakes such as the 1994 Northridge earthquake (Chavez and Binder, 1996) and the 2010 Chile earthquake (Miranda et al., 2012).

Generalized SLFs

To facilitate the use of the SLFs for similar case studies in other studies beyond the current one, the obtained SLFs were normalized by the total repair cost for each story, as shown in Figure 11, which can be formalized in Equation 1:

$$E\left[\tilde{L} \mid NC \cap R, PSD \vee PFA\right]_{PG,i} = \frac{E[\mathrm{L} \mid NC \cap R, PSD \vee PFA]_{PG,i}}{\sum_j E[\mathrm{L} \mid NC \cap R, \infty]_{PG,j}} \tag{1}$$

where $E\left[\tilde{L} \mid NC \cap R, \ PSD \vee PFA\right]_{PG,\mathrm{i}}$ is the generalized expected repair cost of a particular PG (PSD or ($\vee$) PFA-sensitive) and $NC \cap R$ simply refers to the assumption that the building has not collapsed, and it is repairable. $E[\mathrm{L} \mid NC \cap R, \ PSD \vee PFA]_{PG,\mathrm{i}}$ is the actual expected repair cost of the PG of interest at a given value of EDP (Figure 12) and $\sum_j E[\mathrm{L} \mid NC \cap R, \infty]_{PG,\mathrm{j}}$ is the repair cost considering all PGs in a single story (Figure 11) at maximum EDP (i.e. maximum repair cost) denoted ∞. Figure 13 presents the generalized SLFs (GSLFs) for the hotel building examined here. This is deemed a handy resource for practitioners since it avoids the need to generate a detailed catalog of damageable components each time, and SLFs such as those developed here can be readily adopted. One needs to evaluate the suitability of this normalized data to their specific context and scale the GSLF up via their specific total repair costs (i.e. $\sum_j E[\mathrm{L} \mid NC \cap R, \infty]_{PG,\mathrm{j}}$) to have a representative set of SLFs. The critical thing to note is that the general trend of how economic losses are accumulated with increasing EDP is logical and representative; the relative value of these losses is then specified by the user when scaling them to their particular case
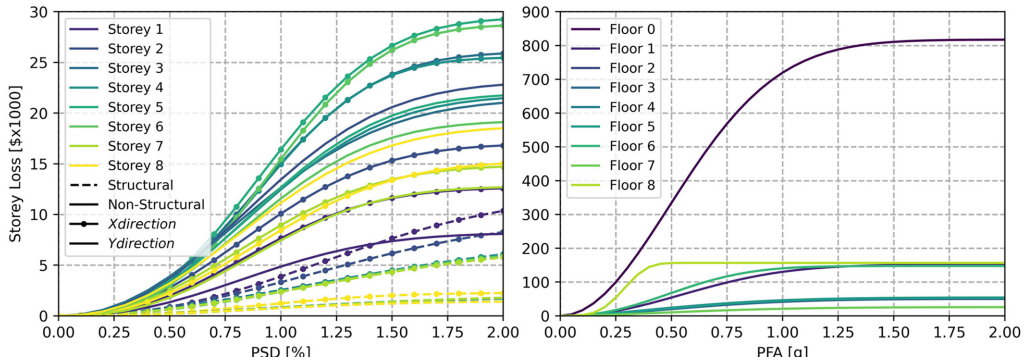
Figure 12. Drift-sensitive and acceleration-sensitive story loss functions.

study. Nevertheless, the limitations should be noted, such as the variability in the components, quantities, and repair costs, which must be evaluated from Table 1. Again, these GSLFs are available as an electronic supplement at OTJ1300607.

Expected annual loss

Estimating losses is crucial for understanding the potential economic impact and consequences to the population in seismically active regions. Moreover, EAL is commonly used in the risk modeling industry and can be computed using various methodologies, such as the FEMA P-58 (2018) methodology developed by the PEER Center. This process, while comprehensive, is computationally intensive and data-heavy, making routine implementation expensive and time-consuming. To streamline this, a simplified approach called story-based loss assessment was introduced by Ramirez and Miranda (2009) and Papadopoulos et al. (2019), which pre-calculates damage estimates and establishes direct relations between EDP and economic losses. This approach eliminates the need for detailed inventory surveys of all building components and specific quantities of each performance group for each story. For instance, the hotel room contents, such as carpets, beds, and furniture, were accounted for as one item sensitive to PFA and with one approximated repair cost per square meter. In this manner, the total replacement cost of each story is distributed among a performance group using readily available information according to building occupancies. Moreover, all damageable components are assigned fragility and loss functions, addressing potential underestimation of losses by assuming non-damageable components. Loss functions are normalized by replacement cost, negating the need for inflation adjustments. Fragility and loss functions are combined before loss assessment to create EDP-to-normalized-loss functions, which can be reused across various floors or even between similar projects. This streamlines data tracking and computation, aiding design professionals in making informed decisions during the design or assessment when building inventory details are often uncertain.

SLFs facilitate the computation of EAL without losing considerable precision (Shahnazaryan et al., 2021), hence their implementation in the present case study. EAL was calculated by integrating site hazard with the structure's vulnerability function (Equation 2), which describes the amount required to repair earthquake damage:
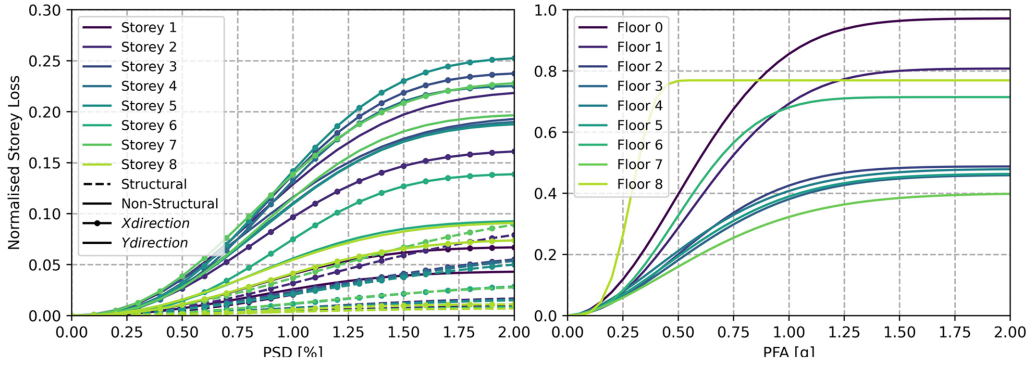
Figure 13. Generalized drift-sensitive and acceleration-sensitive story loss functions.

$$EAL = {}^E[L_T \mid IM] \left| \frac{dH(IM > im)}{\dim} \right| \dim \tag{2}$$

$$E[L_T \mid IM] = E[L \mid NC \cap R, IM](1 - P[D \mid NC, IM])(1 - PC \mid IM)$$
$$+ E[L \mid NC \cap D]P[D \mid NC, IM](1 - PC \mid IM) + E[L \mid C]P[C \mid IM] \tag{3}$$

$E[L_T \mid IM]$ is the expected total economic loss or vulnerability defined in Equation 3 and $H(IM > im)$ describes the site hazard curve's exceedance of a given IM level. The total economic loss is calculated by adding up the costs associated with three distinct, mutually exclusive, and collectively exhaustive events. $E[L \mid NC \cap R, IM]$ is the expected repair cost at a given IM level conditioned on non-collapse and repairability of the building. $E[L \mid NC \cap D]$ is the expected replacement cost at a given IM level conditioned on non-collapse and the non-repairability of the building (i.e. the building has not collapsed, but it is so heavily damaged that it makes more sense to demolish it and rebuild) and is assumed here to be the replacement value of the building. $E[L \mid C]$ is the expected replacement cost due to collapse, also assumed to be the replacement value of the building. $P[D \mid NC, IM]$ is the probability of requiring to demolition given non-collapse of the building at a given IM level due to excessive RPSD, shown in Figure 9. The RPSD demolition limit was assumed to be lognormally distributed with a median of 1.5% and a logarithmic standard deviation of 0.3 as recommended by Ramirez and Miranda (2012). $P[C \mid IM]$ is the collapse probability at a given IM level, obtained from Figure 10.

To compute the $E[L \mid NC \cap R, IM]$, the results of the MSA are used to fit EDP distributions for a wide range of IMs. These functions now become inputs for the SLF, therefore relating an expected loss when the structure has not collapsed and is repairable with an IM, as described by Shahnazaryan and O'Reilly (2021), or expressed as Equation 4 for the entire building:

$$E[L_T \mid NC \cap R, IM] = \sum_i \sum_{PG} E[L_T \mid NC \cap R, PSD(IM) \lor PFA(IM)]_{PG, i} \tag{4}$$

The total replacement cost or $E[L \mid C]$ in Equation 3 was estimated by multiplying a surveyed replacement cost per square meter. Local experts estimated this to be 995.77 USD \$/m^2 and includes demolition costs. This unit value is then multiplied by the total area of the
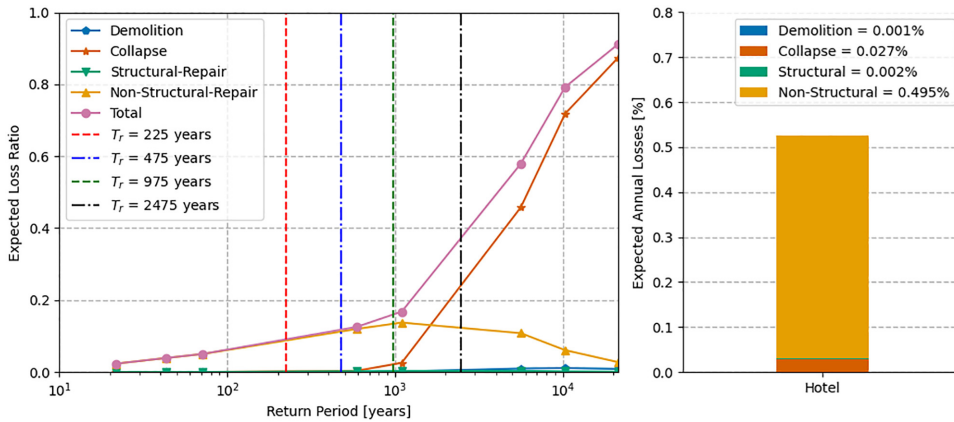
Figure 14. Vulnerability function and expected annual loss with the different contributions disaggregated.

central block, including the underground floor area, which was computed as 6458.69 m^2 to give a total replacement cost of $E[\text{L} \mid C] = \$6.431\text{M}$.

Figure 14 presents the vulnerability function of the hotel first in terms of the expected loss ratio at different return periods, which was normalized with total replacement cost and disaggregated for collapse, demolition, and structural and non-structural repair loss contributions. For the present case, contents are included in the nonstructural repair category. Moreover, from the contribution of each case to the vulnerability, it is possible to note that non-structural losses have the highest contribution for low intensities and collapse for higher intensities. Demolition and structural repair costs are nearly negligible. The former observation may be an indirect consequence of the residual drift threshold used to identify the situations where demolition would be required being too high. These median and dispersion values were developed for a different context and not for the specific case of Ecuador; hence, more refined studies may be performed in the future. Similarly, it may be that the collapse vulnerability of this hotel structure was notably high; hence, many situations where a building would normally be damaged but not collapse and require demolition, did in fact collapse for this particular structure. Compared to Martins and Silva (2021), for example, vulnerability data for a similar typology called CR_LWAL-DUM_H:7, according to Global Earthquake Model foundation taxonomy, means a seven stories high (H:7) reinforced concrete (CR) building with medium ductility (DUM) shear walls (LWAL); slightly higher values for the expected losses of the present case study were found but were within the same overall range.

Figure 14 also presents the contributions to the EAL, which was computed to be 0.525% for this hotel building in Quito. The losses are dominated by the NSE contribution at lower intensities. It was reported that following previous low-intensity ground motions (i.e. $3 < M_w < 5$) in the region, infill cracks were found during field inspections of the hotel building, and repairs were then carried out as general maintenance, which was also observed for the case of Japan and is discussed in O'Reilly et al. (2023). This supports some of the observations presented here regarding the contributions of NSEs to losses in Figure 14 and shows how minor damage like this continuously over a long period is the primary driver of economic losses in buildings. Compared to other values in the literature,
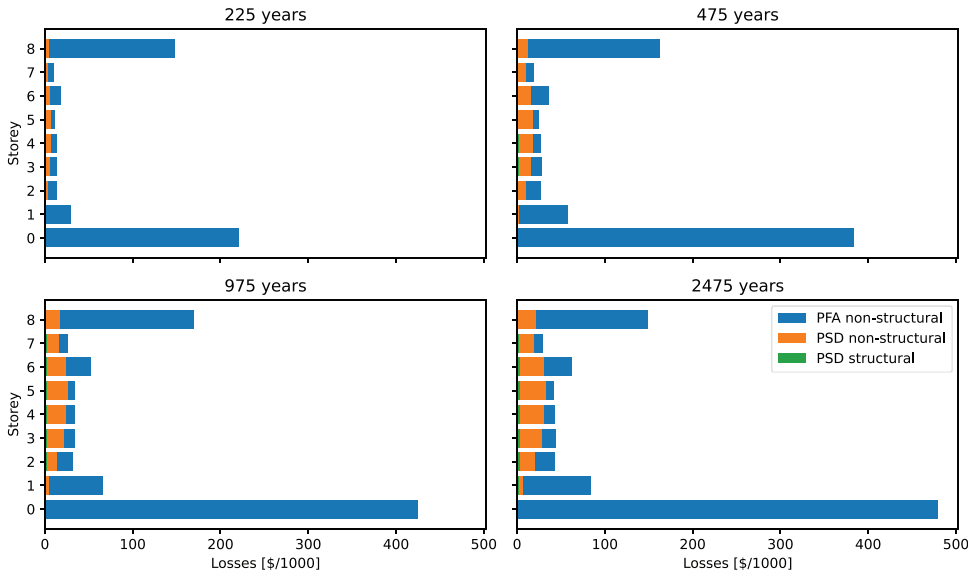
Figure 15. Story repair losses at different return periods.

the EAL for an 8-story moment frame with no structural walls presented by Ramirez et al. (2012) showed a variation between 0.95% and 1.3%, which is higher. Still, it must be recalled that the study from Ramirez et al. (2012) considered structures at a site with higher seismicity. Similarly, the EAL observed here aligns with values observed in Italian structures, as per O'Reilly and Sullivan (2018).

Figure 15 illustrates the disaggregation of repair losses for each of the eight stories, categorized by EDP, and for four return periods, which are commonly referred to as the Design Earthquake and Maximum Considered Earthquake for new and existing structures. Notably, a significant impact of NSE on losses is observed, particularly on the ground floor and the top floor. The losses sensitive to PSD might be overshadowed by the significantly higher repair costs associated with PFA-sensitive losses. It is important to recall that contents are assumed to be PFA-sensitive, expensive elevator equipment on the eighth floor, and costly hotel equipment on the ground floor. For the 2475 return period, it is possible to note how the PSD-sensitive losses spike in floors 2 to 6 where a higher density of infill walls is expected to collapse.

Repair losses, mainly characterized by non-structural losses, add up to $478 K, $765 K, $873 K, and $975 K, respectively, for each return period. These results highlight the importance and need for NSE retrofitting. Furthermore, a more refined analysis as mentioned in O'Reilly et al. (2023) may help adjust NSE fragilities, losses, and retrofit priorities according to owners' recovery objectives. Collapse losses, as depicted in Figure 14, show minimal incidence for the first three studied return periods, emphasizing the significance of a retrofit strategy and its potential to mitigate losses significantly.

Summary and conclusion

This article presented a case study assessment of a hotel building in Quito, Ecuador, built in the late 1950s. The study involved extensive field surveys, material testing, and

monitoring ambient noise vibrations to create a nonlinear numerical model for a comprehensive seismic assessment. It also included a thorough seismic hazard analysis using state-of-the-art methods to select appropriate ground motion records for numerical analysis. This analysis captures the EDPs necessary for estimating repair costs and economic losses. These losses were estimated via a catalog of damageable components based on input from surveys, building owner's information and local experts' input, complete with corresponding fragilities and repair cost data to build SLFs, which were then normalized for general use. The research concludes by presenting structural fragilities according to ASCE/SEI 41-17 (2017) criteria and calculates vulnerability and EALs, providing valuable insights for decision-makers. The main conclusions of this study are as follows:

- Comprehensive seismic assessment relies heavily on information from various sources, in this case, in-situ tests, ambient noise vibrations, and local expert knowledge. Dynamic property correspondence, such as modal shapes and decoupled responses from adjacent buildings, was useful to provide a degree of confidence to the numerical modeling assumptions made.
- BIM emerged as a valuable tool for crafting the damageable inventory and subsequent categorization for simpler handling and future reference. Expanding applications from BIM and automation may help permeate detailed assessment in engineering practice.
- The detailed loss assessment capitalized on the advantages of the SLFs, offering reliable quantifications. Furthermore, GSLF has the potential to extend its applicability widely, making it another remarkable contribution.
- The hotel's performance was noted to fall below contemporary standards such as ASCE/SEI 7-16 (2017) for new structures but satisfies these same standards when assessed as an existing structure. This is a challenge commonly faced by practitioners in the region, where local codes make no distinction between existing and new structures' assessment intensity levels. Decision-makers must assess its collapse probability under the country's standard and their own risk objectives.
- The vulnerability and loss assessment not only estimates decision values but also identifies key contributors, enabling the development of strategic retrofit solutions.

In conclusion, the findings of this case study serve as a valuable reference point for performing seismic loss assessments on structures that do not meet code compliance standards, particularly within Ecuador and the broader South American context. In essence, this research can contribute to informed decision-making regarding the seismic retrofitting of buildings and similarly vulnerable structures in this region.

Funding

ORCID iD

Jose Poveda (iD) https://orcid.org/0000-0002-4990-7207
Gerard J O'Reilly (iD) https://orcid.org/0000-0001-5497-030X

Data and resource availability

All data utilized in this study are available via the electronic supplement, which can be found at https://gerardjoreilly.github.io/publications/.

References

ACI Committee 318 (2019) *Building Code Requirements for Structural Concrete (ACI 318–19) and Commentary (ACI 318R-19)*. American Concrete Institute.

American Society of Civil Engineers (ASCE)/SEI 7-16 (2017) *Minimum Design Loads and Associated Criteria for Buildings and Other Structures*. Reston, VA: ASCE.

American Society of Civil Engineers (ASCE)/SEI 41-17 (2017) *Seismic Evaluation and Retrofit of Existing Buildings*. Reston, VA: ASCE.

Ancheta TD, Darragh RB, Stewart JP, Seyhan E, Silva WJ, Chiou BS-J, Wooddell KE, Graves RW, Kottke AR, Boore DM, Kishida T and Donahue JL (2014) NGA-West2 database. *Earthquake Spectra* 30(3): 989–1005.

Baker JW (2011) Conditional mean spectrum: Tool for ground-motion selection. *Journal of Structural Engineering: ASCE* 137(3): 322–331.

Baker JW (2015) Efficient analytical fragility function fitting using dynamic structural analysis. *Earthquake Spectra* 31(1): 579–599.

Beauval C, Marinière J, Yepes H, Audin L, Nocquet J-M, Alvarado A, Baize S, Aguilar J, Singaucho J-C and Jomard H (2018) A new seismic hazard model for Ecuador. *Bulletin of the Seismological Society of America* 108: 1443–1464.

Calabrese A, Almeida JP and Pinho R (2010) Numerical issues in distributed inelasticity modeling of RC frame elements for seismic analysis. *Journal of Earthquake Engineering* 14(suppl. 1): 38–68.

Cardone D and Perrone G (2015) Developing fragility curves and loss functions for masonry infill walls. *Earthquakes and Structures* 9(1): 257–279. DOI:10.12989/eas.2015.9.1.000

Chavez CW and Binder B (1996) A hospital as victim and responder: The Sepulveda VA Medical Center and the Northridge earthquake. *Journal of Emergency Medicine* 14(4): 445–454.

Cruz C and Miranda E (2021) Damping ratios of the first mode for the seismic analysis of buildings. *Journal of Structural Engineering: ASCE* 147(1): 04020300.

Dávalos H and Miranda E (2019) Evaluation of the scaling factor bias influence on the probability of collapse using $Sa(T1)$ as the intensity measure. *Earthquake Spectra* 35(2): 679–702.

Eads L, Miranda E and Lignos DG (2015) Average spectral acceleration as an intensity measure for collapse risk assessment. *Earthquake Engineering & Structural Dynamics* 44(12): 2057–2073.

Federal Emergency Management Agency (FEMA) P-58 (2018) *Seismic Performance Assessment of Buildings*. Washington, DC: FEMA.

Jalayer F (2003) *Direct Probabilistic Seismic Analysis: Implementing Non-Linear Dynamic Assessments*. Stanford, CA: Department of Civil and Environmental Engineering, Stanford University.

Kijewski-Correa T and Pirnia JD (2007) Dynamic behavior of tall buildings under wind: Insights from full-scale monitoring. *Structural Design of Tall and Special Buildings* 16(4): 471–486.

Kohrangi M, Kotha SR and Bazzurro P (2018) Ground-motion models for average spectral acceleration in a period range: Direct and indirect methods. *Bulletin of Earthquake Engineering* 16(1): 45–65.

McCormick J, Aburano H, Ikenaga M and Nakashima M (2008) Permissible residual deformation levels for building structures considering both safety and human elements. In: *Proceedings of the 14th world conference on earthquake engineering*, Beijing, China, 12–17 October.

Mander JB, Priestley MJN and Park R (1988) Theoretical stress-strain model for confined concrete. *Journal of Structural Engineering: ASCE* 114(8): 1804–1826.

Martins L and Silva V (2021) Development of a fragility and vulnerability model for global seismic risk analyses. *Bulletin of Earthquake Engineering* 19(15): 6719–6745.

Miranda E, Mosqueda G, Retamales R and Pekcan G (2012) Performance of nonstructural components during the 27 February 2010 Chile Earthquake. *Earthquake Spectra* 28(suppl. 1): S453–S471.

Nafeh AMB and O'Reilly GJ (2023) Simplified pushover-based seismic loss assessment for existing infilled frame structures. *Bulletin of Earthquake Engineering* 22: 951–995.

NEC-15 (2014) *Norma Ecuatoriana de la Construcción—NEC: NEC—E—S—Peligro Sísmico/Diseño Sismo Resistente*. Ministerio de Desarrollo Urbano y Vivienda.

O'Reilly GJ and Sullivan TJ (2018) Probabilistic seismic assessment and retrofit considerations for Italian RC frame buildings. *Bulletin of Earthquake Engineering* 16(3): 1447–1485.

O'Reilly GJ, Hasegawa K, Shahnazaryan D, Poveda J, Fukutomi Y, Kusaka A and Nakashima M (2023) On the fragility of non-structural elements in loss and recovery: Field observations from Japan. *Earthquake Engineering & Structural Dynamics* 53: 1125–1144.

Pagani M, Monelli D, Weatherill G, Danciu L, Crowley H, Silva V, Henshaw P, Butler L, Nastasi M, Panzeri L, Simionato M and Vigano D (2014) OpenQuake engine: An open hazard (and risk) software for the global earthquake model. *Seismological Research Letters* 85(3): 692–702.

Papadopoulos AN, Vamvatsikos D and Kazantzi AK (2019) Development and application of FEMA P-58 compatible story loss functions. *Earthquake Spectra* 55(1): 95–112.

Ramirez CM and Miranda E (2009) *Building-Specific Loss Estimation Methods & Tools for Simplified Performance-Based Earthquake Engineering*.

Ramirez CM and Miranda E (2012) Significance of residual drifts in building earthquake loss estimation. *Earthquake Engineering & Structural Dynamics* 41(11): 1477–1493.

Ramirez CM, Liel AB, Mitrani-Reiser J, Haselton CB, Spear AD, Steiner J, Deierlein GG and Miranda E (2012) Expected earthquake damage and repair costs in reinforced concrete frame buildings. *Earthquake Engineering & Structural Dynamics* 41(11): 1455–1475.

Scott MH and Fenves GL (2006) Plastic hinge integration methods for force-based beam–Column elements. *Journal of Structural Engineering: ASCE* 132(2): 244–252.

Shahnazaryan D and O'Reilly GJ (2021) Integrating expected loss and collapse risk in performance-based seismic design of structures. *Bulletin of Earthquake Engineering* 19(2): 987–1025.

Shahnazaryan D, O'Reilly GJ and Monteiro R (2021) Story loss functions for seismic design and assessment: Development of tools and application. *Earthquake Spectra* 37(4): 2813–2839.

Taghavi S and Miranda E (2003) *Response assessment of nonstructural building elements*. PEER report 2003-05, 5 January. Berkeley, CA: Pacific Earthquake Engineering Research Center (PEER), University of California, Berkeley.

Tamura Y, Yoshida A and Zhang L (2004) *Evaluation Techniques of Damping in Buildings*. Council on Tall Buildings and Urban Habitat, pp. 158–165.

Vamvatsikos D and Cornell CA (2002) Incremental dynamic analysis. *Earthquake Engineering & Structural Dynamics* 31(3): 491–514.